

# Real-Time Phase and Task Estimation for Controlling a Powered Ankle Exoskeleton on Extremely Uneven Terrain

Roberto Leo Medrano, *Student Member, IEEE*, Gray Cortright Thomas, *Member, IEEE*, Elliott J. Rouse, *Senior Member, IEEE* and Robert D. Gregg, *Senior Member, IEEE*

**Abstract**— Positive biomechanical outcomes have been reported with emerging lower-limb exoskeletons in laboratory settings, but the control of these exoskeletons in uncertain environments outside of the laboratory remains a challenging problem. Human locomotion frequently involves dynamic, non-steady-state tasks, but state-of-the-art exoskeleton controllers have difficulty delivering appropriate assistance in synchrony with the human gait as the task or rate of phase progression change. In this paper we present a torque controller for an ankle exoskeleton that uses state estimation with a data-driven kinematic model to continuously estimate the phase, phase rate, stride length, and ramp parameters during locomotion. The controller applies torque assistance based on the estimated phase and adapts the torque profile based on the estimated ramp and stride length to match human torques observed in a multi-activity database of 10 able-bodied human subjects. We demonstrate *in silico* that the controller yields phase estimates that are significantly more accurate than the state of the art, while also estimating task variables with comparable accuracy to recent machine learning approaches. We also show that the inclusion of ramp angle estimates significantly improves phase estimation. The controller implemented in an ankle exoskeleton successfully adapts its assistance in response to changing phase and task variables, both during controlled treadmill trials and in a real-world stress test with extremely uneven terrain. This technical advancement will enable the field to study various biomechanical outcomes associated with exoskeletons outside of the laboratory.

**Index Terms**— exoskeleton, Kalman filter, control, phase

## I. INTRODUCTION

Robotic exoskeletons may someday allow us to overcome the limits of our natural bodies. Emerging lower-limb exoskeletons are capable of providing assistive joint torques to help their wearers walk and carry loads with promising outcomes such as reduced metabolic cost [1]–[5] and muscle effort [6]–[8]. Most research to date has focused on steady-state locomotion in a controlled laboratory setting, where the task and rate of phase progression (through the gait cycle) are nearly constant. This makes it easier to design control strategies that deliver appropriate torque assistance in synchrony with the user’s gait. However, control strategies based on these assumptions do not perform well outside of the laboratory, where environments are uncertain and locomotion is highly non-steady and transitory. In order for the field to study biomechanical outcomes outside of the laboratory, new control strategies are needed that explicitly account for continuously varying task and phase.

During steady-state locomotion in controlled laboratory settings, phase progression can be reasonably predicted by time normalized

This work was supported by the National Institute of Child Health & Human Development of the NIH under Award Number R01HD094772 and by the D. Dan and Betty Kahn Foundation. The content is solely the responsibility of the authors and does not necessarily represent the official views of the NIH.

R. L. Medrano and E. J. Rouse are with the Department of Mechanical Engineering and the Robotics Institute, University of Michigan, Ann Arbor, MI 48109. G. C. Thomas and R. D. Gregg are with the Department of Electrical Engineering and Computer Science and the Robotics Institute, University of Michigan, Ann Arbor, MI 48109. Contact: {leomed, gcthomas, ejrouse, rdgregg}@umich.edu

by the stride period. The stride period is usually estimated as the time between previous ipsilateral heel strike (HS) events, which can reasonably predict the next HS event during steady locomotion. This ‘timing-based’ approach is quite effective and widely used for controlling exoskeletons on treadmills [9]. Typically this phase estimate parameterizes a pre-defined torque profile to deliver real-time assistance through the exoskeleton’s actuator(s). Recent work has demonstrated impressive reductions in the metabolic cost of level-ground treadmill walking by optimizing this torque profile in real-time [2], [3]. While this paradigm of timing-based estimation (TBE) for torque control works well in steady-state locomotion, it is not designed for more practical conditions outside the laboratory where both the periodicity of gait and the task can change on the fly.

Recent work has addressed the problem of *non-constant* phase progression in powered prostheses and orthoses by introducing phase-based<sup>1</sup> controllers [10]–[15], which continuously adjust the rate of phase progression to accommodate dynamic speed changes mid-stride. In contrast to the timing-based approach, these controllers estimate the gait phase online using the exoskeleton’s sensors. This phase can be estimated from shank [10] or thigh motion [11], e.g., the global angle versus its velocity or integral. Alternatively, Thatte *et al.* recently introduced an Extended Kalman Filter (EKF) to estimate phase and its derivative (phase rate) without relying on any particular sinusoidal pattern in the sensors [16]. This EKF was also shown to yield more accurate phase estimates in non-steady locomotion when compared to conventional timing- and EMG-based controllers. Building on this result, we pursue further improvements in phase estimation by incorporating other variations in task beyond speed.

To handle transitions between tasks, several groups have proposed solutions rooted in machine learning classifiers. Such classifiers can detect the human’s intended task from patterns in the exoskeleton’s sensor signals in order to apply the correct task-specific controller (e.g., stair ascent vs. level-ground walking) [9], [14], [17]–[22]. While this approach can identify discrete changes in task, it is less ideal for detecting continuous variations within a family of tasks or handling tasks outside the training data. Recently developed gait models have introduced task variables such as ground slope or stair height that continuously parameterize the instantaneous task [23], [24]. These variables capture more of the task’s features, and can thus provide more tailored assistance to the user. Controllers based on these models have been limited to measuring the task parameter only once per stride [24]—similar to the rate of phase progression before phase-based controllers were introduced. A notable exception to this paradigm is the work of Holgate *et al.* [10], which exploited the relation in the phase plane between tibia angle and angular velocity to continuously estimate gait phase and stride length. However, this relation does not hold for non-steady-state walking, nor does it extend to other joints or task variables (e.g., ground inclination). Recent work has also combined ambulation mode classification with continuous

<sup>1</sup>We define ‘phase-based’ approaches as those where the rate of phase progression can change continuously within a stride, whereas ‘timing-based’ approaches have a fixed rate over the stride. Note that both would fall under the category of ‘phase-based’ approaches according to [9].

task variable estimates for ramp incline, step height, and walking speed [25], but this approach uses multiple EMG electrodes, IMUs, and goniometers that may not be available onboard an exoskeleton.

This paper introduces an Extended Kalman Filter (EKF)-based exoskeleton controller that continuously learns both the phase state (phase and phase rate) and task state (ramp and stride length) to modulate the torque profile of an assistive ankle exoskeleton in a biomimetic fashion. The EKF can indirectly estimate the gait and task parameters in real time using onboard sensors, letting the controller adapt its output quickly and in response to a continuously-varying environment. The contributions of our work include 1) introducing a new EKF phase estimator that also estimates task parameters in continuous time, 2) validating the quality of the state vector estimates using a leave-one-out cross validation based on previously-collected motion capture data of 10 able-bodied subjects walking on various inclines at various speeds, 3) validating the EKF estimates on an ankle exoskeleton in a controlled lab environment on an instrumented treadmill which can vary speed and inclination, and 4) validating the EKF estimates on an ankle exoskeleton in an outside setting during free-walking on a continuously varying surface (the Michigan Wave Field). This contribution to exoskeleton control is important since practical, real-world usage of exoskeletons will require controllers that adapt their assistance during walking at non-steady-state conditions within a continuously evolving task.

## II. MODELLING AND ESTIMATING GAIT

### A. Gait Model

We consider the control of an ankle exoskeleton that measures global shank and global foot angles and applies ankle torque to assist the wearer in periodic walking with variability in the stride timing, ramp angle, and stride length. To account for such variability, we define the gait-state vector  $x$  as

$$x(t) = (p(t) \quad \dot{p}(t) \quad l(t) \quad r(t))^T, \quad (1)$$

comprising a phase (or normalized time) signal  $p$ , its time derivative  $\dot{p}$ , a stride length signal  $l$ , and a ramp angle signal  $r$ . The phase variable ranges from 0 to 1 and increases monotonically throughout strides, resetting at ipsilateral heel-strokes. We express the global shank angle  $\theta_s$  and global foot angle  $\theta_f$  (see Fig. 1) as a time-invariant function of the gait state,

$$\begin{pmatrix} \theta_s(t) \\ \theta_f(t) \end{pmatrix} = \begin{pmatrix} h_f(x(t)) \\ h_s(x(t)) \end{pmatrix} = h(x(t)). \quad (2)$$

We use global angles, as opposed to joint angles, because of the convenient relationship between global foot angle and ramp inclination during stance, and because they can be measured directly with IMUs.

**1) Constrained Least-squares Regression:** The model  $h(x)$  was generated using labeled training data from a 10-subject able-bodied dataset [23]. This dataset contains walking data grouped by strides, over a range of speeds (0.8, 1, and 1.2 m/s) and ramps (-10 to 10 degree inclination in increments of 5 degrees). Each stride features 150 samples of kinematic and kinetic data, from which we calculated phase progression over the stride. Thus the dataset provided labeled tuples of  $(\theta_s(t), \theta_f(t), x(t))$  for all ( $>25,000$ ) individual strides.

We used constrained least-squares optimization to regress models of the foot and shank angles as a function of the gait-state vector  $x$ . We structured our model of  $h(x)$  as a linear function of a constant parameter vector  $\phi \in \mathbf{R}^{64 \times 2}$  and a regressor row vector  $R : \mathbf{R}^4 \mapsto \mathbf{R}^{1 \times 64}$  as

$$h(x) = \phi^T R^T(x). \quad (3)$$

Our regression minimized the sum squared error for the equation

$$(\theta_s(t) \quad \theta_f(t)) = R(x(t))\phi, \quad (4)$$

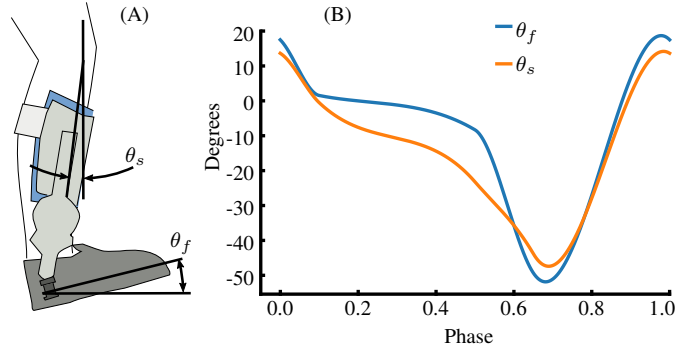


**Fig. 1.** (A) A sagittal-plane view of the human leg. The foot angle  $\theta_f$  is defined from the global horizontal, and the shank angle  $\theta_s$  is defined from the global vertical. (B) Average  $\theta_f$  and  $\theta_s$  profiles at zero ramp and at 1 m/s over the gait cycle.

over all the tuples  $(\theta_s(t), \theta_f(t), x(t))$  in the dataset.

The regressor row  $R(x)$  is structured with a series of Kronecker products<sup>2</sup> of simpler row-vector functions of  $x$  as

$$R(x) = B_p(p) \otimes \Lambda_r(r) \otimes \Lambda_l(l) \otimes \Lambda_p(p), \quad (5)$$

where the components are as follows:

- The Boolean selector row  $B_p(p) : \mathbf{R} \mapsto \mathbf{R}^{1 \times 4}$ , defined as

$$B_p(p) = \begin{cases} (1, 0, 0, 0) & \text{if } 0 \leq p \leq 0.1, \\ (0, 1, 0, 0) & \text{if } 0.1 < p \leq 0.5, \\ (0, 0, 1, 0) & \text{if } 0.5 < p \leq 0.65, \\ (0, 0, 0, 1) & \text{if } 0.65 < p \leq 1, \end{cases} \quad (6)$$

divides the gait phase into four sections for the purpose of piece-wise polynomial modelling. The sections were determined by inspection of the nominal bio-mechanical kinematics in our dataset.

- The ramp angle polynomial basis  $\Lambda_r : \mathbf{R} \mapsto \mathbf{R}^{1 \times 2}$  is a first-order Bernstein basis in ramp angle,

$$\Lambda_r(r) = (r \quad (1-r)), \quad (7)$$

which allows for continuous adjustment to ground slope.

- The stride length polynomial basis  $\Lambda_l : \mathbf{R} \mapsto \mathbf{R}^{1 \times 2}$  is another first-order Bernstein basis in stride length,

$$\Lambda_l(l) = (l \quad (1-l)), \quad (8)$$

which similarly allows for kinematic changes associated with step length.

- The phase-polynomial basis  $\Lambda_p : \mathbf{R} \mapsto \mathbf{R}^{1 \times 4}$  is a Bernstein polynomial basis, defined as

$$\Lambda_p(p) = ((1-p)^3 \quad 3(1-p)^2p \quad 3(1-p)p^2 \quad p^3). \quad (9)$$

**2) Least-squares Constraints:** To ensure desirable properties, including continuity of the function  $h(x)$  (the global foot and shank angle predictions), the elements of the parameter matrix  $\phi$  are subject to constraints. The constraints guarantee that the  $h(x)$  function 1) predicts constant-with-phase behavior if stride length is zero, 2)

<sup>2</sup>The Kronecker product of row-vectors  $A \in \mathbf{R}^{1 \times N}$  and  $B \in \mathbf{R}^{1 \times M}$ , denoted  $A \otimes B \in \mathbf{R}^{1 \times NM}$ , is the block row-vector  $(a_1B \quad a_2B \quad \dots \quad a_NB)$ . For matrices  $A \in \mathbf{R}^{n \times N}$ ,  $B \in \mathbf{R}^{m \times M}$ , this generalizes to

$$A \otimes B = \begin{pmatrix} a_{11}B & a_{12}B & \dots & a_{1N}B \\ a_{21}B & a_{22}B & \dots & a_{2N}B \\ \vdots & \vdots & \ddots & \vdots \\ a_{n1}B & a_{n2}B & \dots & a_{nN}B \end{pmatrix} \in \mathbf{R}^{nm \times NM}.$$

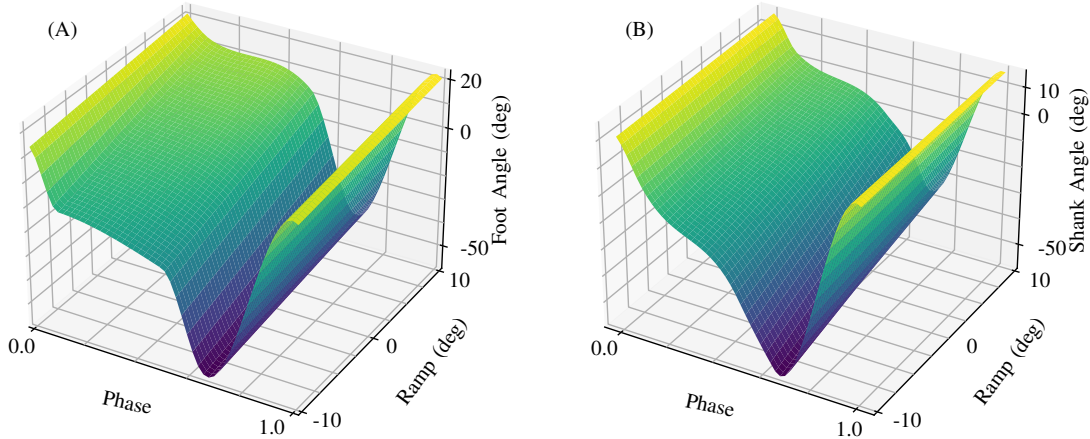


**Fig. 2.** The regressed continuous gait models for  $\theta_f$  and  $\theta_s$ . As the models themselves depend on three variables ( $p$ ,  $l$ , and  $r$ ), they are difficult to express in 3D-space. In this figure, the model relation between phase and ramp is shown (with stride length constant at 1 meter). Stride length merely changes the amplitudes of the gait model.

predicts the global foot angle is equal to the ramp angle when stride length is zero or when phase takes the value 0.2, and 3) is guaranteed to provide  $C^1$  continuity in phase.

We first define a set of two constraints to ensure constant-with-phase behavior when stride length is zero, i.e., when the person is standing still. The first constraint concerns the case where both stride length  $l$  and ramp angle  $r$  are zero. In this case, we expect both global foot  $\theta_f$  and global shank  $\theta_s$  angles to be zero, which we express using the following matrix equality:

$$\underbrace{I_4}_{\forall B_p(p), \text{ if } r=0 \text{ and } l=0,} \otimes \underbrace{\Lambda_r(0) \otimes \Lambda_l(0)}_{\forall p} \otimes \underbrace{\begin{pmatrix} \Lambda_p(0) \\ \Lambda_p(\frac{1}{4}) \\ \Lambda_p(\frac{1}{2}) \\ \Lambda_p(\frac{3}{4}) \end{pmatrix}}_{\text{both angles are zero}} \phi = \underbrace{0 \in \mathbf{R}^{16 \times 2}}, \quad (10)$$

where any four representative phases would have the same effect of constraining the polynomial in phase to be constant, so long as they were linearly independent.

The second constraint concerns the case where the ramp angle is non-zero and the stride length is zero. In this case, the shank is vertical and the foot is aligned with the ramp. Since our model is linear in ramp angle, we only need to apply one constraint, and any ramp angle choice will work. We choose the particular condition of  $l = 0$  and  $r = 10$  and apply the constraint

$$\underbrace{I_4}_{\forall B_p(p), \text{ if } r=10 \text{ and } l=0,} \otimes \underbrace{\Lambda_r(10) \otimes \Lambda_l(0)}_{\forall p} \otimes \underbrace{\begin{pmatrix} \Lambda_p(0) \\ \Lambda_p(\frac{1}{4}) \\ \Lambda_p(\frac{1}{2}) \\ \Lambda_p(\frac{3}{4}) \end{pmatrix}}_{\theta_f=10, \theta_s=0} \phi = \underbrace{(10 \ 0) \otimes 1_{16 \times 1}}_{\forall r, l}. \quad (11)$$

Through a similar mechanism, we constrain the model to predict that regardless of stride length, the foot angle will be equal to  $r$  at  $p = 0.2$  to represent flat-foot contact. We express this constraint on

the foot using the following equality:

$$\left[ \underbrace{B_p(0.2)}_{\text{at } p=0.2,} \otimes \underbrace{\begin{pmatrix} \Lambda_r(0) \\ \Lambda_r(10) \end{pmatrix}}_{\forall r} \otimes \underbrace{I_2}_{\forall l} \otimes \underbrace{\Lambda_p(0.2)}_{\text{at } p=0.2} \right] \phi = \underbrace{\begin{pmatrix} 1 \\ 0 \end{pmatrix}}_{\theta_f=r} \quad (12)$$

$$= \underbrace{(0 \ 0 \ 10 \ 10)^T}_{\in \mathbf{R}^{4 \times 1}},$$

where we use the conditions  $r = 0$  and  $r = 10$  without loss of generality for clarity of presentation.

To express the  $C^0$  continuity of the model, we require  $\lim_{p \rightarrow \rho^-} h(x) = \lim_{p \rightarrow \rho^+} h(x)$  for all  $0 < \rho < 1$  as well as the special wrap-around case where  $\lim_{p \rightarrow 1^-} h(x) = \lim_{p \rightarrow 0^+} h(x)$ . This is trivially satisfied everywhere except at  $p = 0.1, 0.5, 0.65$ , and in the wrap-around case. In these four cases, equality constraints must be satisfied for all possible stride lengths and ramp angles. We can express this constraint on  $\phi$  using a matrix equality:

$$\left( \underbrace{\begin{pmatrix} 1 & -1 & 0 & 0 \end{pmatrix}}_{\text{comparing adjacent gait sections}} \otimes \underbrace{I_2}_{\forall r} \otimes \underbrace{I_2}_{\forall l} \otimes \underbrace{\Lambda_p(0.1)}_{\forall p} \right) \phi = \underbrace{0 \in \mathbf{R}^{16 \times 2}}_{(0 \ 0 \ 0 \ 1) \otimes I_2 \otimes I_2 \otimes \Lambda_p(1) - (1 \ 0 \ 0 \ 0) \otimes I_2 \otimes I_2 \otimes \Lambda_p(0)}. \quad (13)$$

To express the  $C^1$  continuity constraint, we exploit the linearity of the Kronecker product. For almost all  $p$  we can express the derivative

$$\frac{dh^T(x)}{dp} = \left[ B_p(p) \otimes \Lambda_l(l) \otimes \Lambda_r(r) \otimes \frac{d\Lambda_p(p)}{dp} \right] \phi, \quad (14)$$

since  $\frac{dB_p(p)}{dp}$  is zero almost everywhere. Note that  $d\Lambda_p/dp : \mathbf{R} \mapsto \mathbf{R}^{1 \times 4}$  is available analytically. The resulting continuity constraint takes a similar form to the prior,

$$\left( \underbrace{\begin{pmatrix} 1 & -1 & 0 & 0 \end{pmatrix}}_{\forall r, l} \otimes \underbrace{I_4}_{\forall p} \otimes d\Lambda_p/dp(0.1) \right. \otimes \underbrace{I_4}_{\forall p} \otimes d\Lambda_p/dp(0.5) \otimes \underbrace{I_4}_{\forall p} \otimes d\Lambda_p/dp(0.65) \left. \otimes \underbrace{I_4}_{\forall p} \otimes d\Lambda_p/dp(1) - (1 \ 0 \ 0 \ 0) \otimes I_4 \otimes d\Lambda_p/dp(0) \right) \phi = \underbrace{0 \in \mathbf{R}^{16 \times 2}}_{(0 \ 0 \ 0 \ 1) \otimes I_4 \otimes d\Lambda_p/dp(1) - (1 \ 0 \ 0 \ 0) \otimes I_4 \otimes d\Lambda_p/dp(0)}. \quad (15)$$

**3) Complete Gait Model:** We performed the regressions for the foot and shank angle models using the constrained least-squares optimization function `lsqlin` in MATLAB. The resulting models  $h_f$  and  $h_s$  (Fig. 2) not only described how the foot and shank kinematics varied with phase, but also with ramp and stride length.

### B. Biomimetic Exoskeleton Torque Profile

During the live trials, the exoskeleton provided torque assistance according to a profile parameterized by phase. We regressed this biomimetic torque profile using the biological ankle torques in our dataset such that the profile also continuously varied with stride length and ramp. The regression was performed using a near-identical regressor structure as in (4) with no constraints and with the biological ankle torque in lieu of  $\theta_f$  and  $\theta_s$ . This yielded a torque profile encoded with the same structure as the gait model in (3).

### C. Dynamic Model and State Estimator

**1) Primary Phase EKF Model:** Our EKF-based controller largely uses the standard equations for an Extended Kalman Filter (see Appendix I). We define the state vector as the gait state in (2). The system process is encoded using the state transition matrix  $F$ :

$$F = \begin{bmatrix} 1 & \Delta t & 0 & 0 \\ 0 & 1 & 0 & 0 \\ 0 & 0 & 1 & 0 \\ 0 & 0 & 0 & 1 \end{bmatrix} \quad (16)$$

such that phase is updated by simple numerical integration of phase rate using the time stride  $\Delta t$ .

The state covariance matrix is defined as  $P = 1e^{-3} \times I_{4 \times 4}$ . We define our process noise matrix  $\Sigma_Q$  as a diagonal matrix  $\text{diag}[0, \sigma_{22}^2, \sigma_{33}^2, \sigma_{44}^2] \times \Delta t$ , where  $\sigma_{22}$ ,  $\sigma_{33}$ , and  $\sigma_{44}$  are the standard deviations for  $\dot{p}$ ,  $\dot{l}$ , and  $\dot{r}$ , respectively. Phase  $p$  has no process noise since it is defined using a noiseless integration of  $p$ . The diagonal variances act as tunable parameters that modulate EKF performance; we empirically tuned the performance and found that  $\sigma_{22} = 6e^{-3}$ ,  $\sigma_{33} = 1e^{-2}$ , and  $\sigma_{44} = 3e^{-2}$  yielded good performance.

**2) Measurement Model:** Within the update stride of the EKF, our observation function  $h(x)$  extends the directly measurable variables  $\theta_f$  and  $\theta_s$ . To encode time-dependent measurement information, we also model the velocity of the foot  $\dot{\theta}_f$  and shank  $\dot{\theta}_s$ . These velocities are defined using the differentiation chain rule:

$$\begin{bmatrix} \dot{\theta}_f \\ \dot{\theta}_s \end{bmatrix} = \begin{bmatrix} \frac{\partial \theta_f}{\partial \dot{p}} \\ \frac{\partial \theta_s}{\partial \dot{p}} \end{bmatrix} = \begin{bmatrix} \frac{\partial \theta_f}{\partial p} \\ \frac{\partial \theta_s}{\partial p} \end{bmatrix} \dot{p} \quad (17)$$

where  $\dot{p}$  is the estimate of the phase rate from the prediction stride and the partial derivatives of  $\theta_f$  and  $\theta_s$  are available analytically. The observation function is then  $h'(x) = [\theta_f, \dot{\theta}_f, \theta_s, \dot{\theta}_s]^T$ .

**3) Nonlinear stride length transformation:** Within walking, there exists an upper limit on a person's stride lengths, which is determined by the length of their legs. Additionally, we can choose to model the smallest possible stride length as 0, as negative stride lengths that could model backwards walking are instead handled by positive stride lengths and negative phase rates. To encode these choices, we model the stride length as the output of an arctangent transformation [26], to which the input is a ‘pseudo-stride length’  $l_p$ . The arctangent transformation is defined as:

$$l(l_p) = \frac{2}{\pi} \arctan\left(\frac{\pi}{2} l_p\right) + 1. \quad (18)$$

This saturates the stride length output at 2 (meters) and floors it at 0.  $l_p$  is allowed to vary freely during EKF estimation (Appendix I). Our state vector  $x$  technically contains  $l_p$  instead of  $l$ , but for a

more intuitive understanding of our estimation, we referred to it as containing stride length instead of its ‘pseudo’ counterpart. Within the Jacobian  $H$  in the update step of the EKF, we also pre-multiply all partial derivatives with respect to  $l$  by  $\frac{\partial l}{\partial l_p}$ .

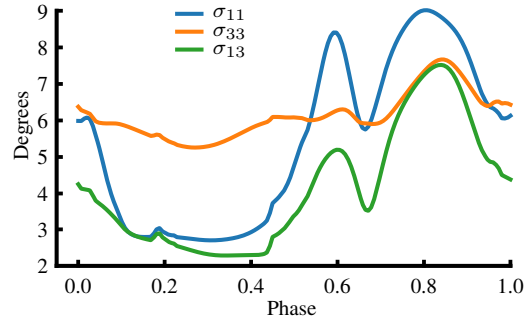


**Fig. 3.** The heteroscedastic measurement noise model as a function of phase. Foot angle variance  $\sigma_{11}$  and its covariance with shank angle  $\sigma_{13}$  are lowest during the flat-foot contact portion of gait, as it acts as a kinematic constraint for all subjects.

**4) Heteroscedastic Noise Model:** EKFs generally encode measurement noise in a *constant*  $\Sigma_R$  matrix. However, this constant model is unable to selectively change the trust in the measurements during regions of the state space where those measurements are known to be informative. For example, we expect that for phase values corresponding to flat-foot contact during locomotion, the measurements of foot angle will be highly informative for the ramp angle, given the position constraint of foot contact. To improve the performance of our phase EKF controller, we implemented a *heteroscedastic* measurement noise matrix, in which the diagonal and off-diagonal elements for foot and shank angle varied with phase. Using the prior dataset, we calculated the covariance matrices (equivalent to  $\Sigma_R$ ) of the measurement residuals  $y$  for the foot and shank angle at each of the 150 sampled phase values within the dataset (see Fig. 3). The resulting model of  $\Sigma_R$  then depends on the value of the phase estimate,

$$\Sigma_R(p) = \begin{bmatrix} r_{11}(p) & 0 & r_{13}(p) & 0 \\ 0 & \sigma_{22,r}^2 & 0 & 0 \\ r_{31}(p) & 0 & r_{33}(p) & 0 \\ 0 & 0 & 0 & \sigma_{44,r}^2 \end{bmatrix} \quad (19)$$

where  $r_{11}$  and  $r_{33}$  are the residual variances for the foot and shank respectively,  $r_{13}$  (equal to  $r_{31}$ ) is the residual covariance between the foot and shank, and  $\sigma_{22,r}$  and  $\sigma_{44,r}$  are constant standard deviations of measurement noise for the foot and shank angular velocities respectively (both empirically tuned to a value of  $60 \frac{\text{deg}}{\text{s}}$ ).

As expected, measurement covariance for the foot and shank angles is lowest during flat-foot contact, where walking gaits experience a position constraint, and grows more uncertain as gait progresses to swing phase, where there is greater variation in kinematics.

### D. Heelstrike-based Estimation Backup

To protect the EKF controller against getting lost in its estimation, we introduced a backup process that was permitted to reset the estimator state in the event of sub-par phase estimation. This backup system uses a similar approach to the conventional “Timing Based Estimation” (TBE, [27]), which detects heel strikes and records the timestamps for each heel strike event. Unlike the conventional TBE approach, our backup plan also records data during the stride in between these heel strike events. For each stride, the system then calculates the phase at each recorded sample by dividing each time

point within the stride by the total stride duration. Phase rate is calculated as a constant: the inverse of stride duration.

To estimate ramp angle and stride length, the backup system formulates a least squares problem using the data collected from the previous stride. At the instant of heel strike, the system solves the least squares problem to estimate the best ramp angle and stride length from the previous stride. As with phase rate, these values are constant for that stride. In this way, the backup system estimates the state vector  $\bar{x}$  over the samples from the previous stride.

If the backup describes a better fit to the subject's kinematics than the EKF, the backup resets the EKF state vector  $x$  with its own backup state vector. The backup system uses its state estimates  $\bar{x}$  from the previous stride to estimate foot and shank angles using the EKF gait model  $h$ , and then computes the sum of squares of the residuals (SSR) using the residual vector  $\bar{y}$  over that stride. It then compares its SSR to the SSR from the phase EKF (calculated using  $y$  from the EKF) over that stride. If the SSR from the backup is sufficiently smaller than the SSR from the EKF, i.e., the EKF is performing poorly, then the backup overrides the EKF and places it back on course.

Unlike our EKF, this backup system cannot estimate the state vector in real time; it can only provide constant stride-length, ramp, and phase rate estimates after each stride. Since it cannot track changes in phase rate, we expect it to under-perform the EKF in most scenarios. In our experiments, we aimed to have under two overrides per trial to ensure that our EKF was performing well.

### III. METHODS

Our experiments address the following hypotheses: H1) Our EKF based controller has a significantly lower phase RMS error compared to phase estimates from a HS-to-HS timing based controller (state-of-the-art) in a leave-one-out cross validation; H2) The inclusion of ramp statistically improves the phase RMS error in a leave-one-out cross validation; and H3) Our real-time EKF estimate of phase has an RMS error less than state-of-the-art timing based estimators in the presence of actuator torques. We also present the result of the EKF working in a practical outdoors setting with exoskeleton actuation. All human participants gave written informed consent with approval from the Medical IRB of the University of Michigan.

#### A. EKF Simulation

We cross-validated our EKF *in silico* using our previously published walking dataset (N=10 subjects [23]). The trials spanned five different ramp angles between -10 and 10 degrees, and three different walking speeds (0.8, 1, and 1.2 m/s). The dataset contains walking data indexed by walking stride, which was used for training the gait model  $h$ . This stride data can be concatenated together to form a continuous walking sequence, which we can then input to our EKF to see how it performs with realistic locomotion. The complete source code for our simulation is available in a ready-to-run computation capsule format through CodeOcean [28].

#### B. Hardware Setup

We implemented our phase EKF on an ankle exoskeleton system (ExoBoot, Dephy, Inc., Maynard, MA) for our live experiments. We used a separate IMU to measure each of the global angles due to the compliance of the exoskeleton's structure. We estimated the global shank angle using a custom attitude EKF that ran concurrently with our phase EKF. The attitude EKF used readings from the onboard IMU (TDK Invensense MPU-9250) mounted above the ankle joint of the exoskeleton. To measure global foot angle, we opted to use a different IMU (3DM-CX5-25, LORD Microstrain) placed on the boot

of the exoskeleton. This IMU estimates global orientation from which we obtained the global foot angle (i.e., pitch angle). For the angular velocity measurements, we measured the shank angular velocity directly using the exoskeleton's gyro readings, and computed foot angular velocity by adding shank velocity to the numerical derivative of the exoskeleton's ankle encoder.

For the indoor hardware experiment, three able-bodied human subjects walked on an instrumented Bertec treadmill with variable belt speed and inclination. The outdoor experiment was conducted with a single able-bodied human subject on the iconic University of Michigan Wave Field (GPS: 42.29322775221383, -83.71167738308422), which gives a prototypical example of extremely unsteady terrain and thus acts as a practical stress test for our EKF.

#### C. Cross-Validation Phase Estimate Quality Experiment (H1)

To identify the ability of our EKF to adapt to new subjects while accurately estimating phase, we performed leave-one-out cross-validation on our EKF-based controller using our dataset, where ground truth phase was calculated using the normalized time between heel-strokes. For each subject, this cross-validation trained a new gait model using the individual stride data from the remaining nine subjects. We then used the concatenated stride walking data from the subject as input to our EKF simulator, and computed the phase root mean squared error (RMSE) of our EKF relative to the ground truth phase measurements for each individual stride across the dataset. To determine the improvement produced by our EKF controller, we compare the stride-wise phase RMSEs against the phase RMSEs from a simulated timing-based estimate (TBE), which predicts the current phase in real-time using the normalized timings of previous heel strikes. This common method is causal whereas ground truth phase is non-causal. We calculate the significance of this improvement using a one-sided paired t-test in which we compare differences in the phase RMSE for each stride within the dataset between the EKF and TBE approaches. We also compute the stride length and incline RMSE relative to the ground truth values from the dataset.

#### D. Measuring the Importance of Ramp Estimation (H2)

In a separate leave-one-out cross validation experiment, we assess the improvement to phase estimation quality that comes from the inclusion of the ramp state in the state vector. The influence of stride length was not separately investigated because its relationship with phase estimation is more obvious due to the correlation between stride length and gait speed. To effectively eliminate the ramp state variable, elements of the process noise matrix  $\Sigma_q$  and covariance matrix  $P$  corresponding to ramp were initialized to extremely low values on the order of  $1e^{-12}$ , which prevented the estimates from changing in real time. These values were not simply set to zero in order to avoid numerical issues in the real-time computation of the state estimate. We then computed the phase RMSE using the phase estimates of this limited EKF and determined the significance of including ramp by comparing the phase RMSE for each stride to those from the EKF again using a paired t-test (as in Sec. III-C).

#### E. Treadmill Test (H3)

We characterized our controller's performance during a controlled treadmill experiment. In this experiment, three able-bodied participants walked with the EKF-controlled exoskeleton for two five-minute segments. In the first segment, participants continuously walked on level ground for thirty seconds at 1.25 m/s, followed by thirty seconds at 1.8 m/s, followed by a return to 1.25 m/s. Then, the treadmill inclined over a period of roughly one minute up to a

maximum of 10 degrees; participants walked uphill at 10 degrees for roughly 50 seconds until the 3.5 minute mark. Finally, participants walked while the treadmill returned to a level ground setting, and walked at level ground until the five-minute duration finished. The second segment was identical to the first, except that instead of the treadmill speeding up to 1.8 m/s it slowed to 0.8 m/s, and instead of the treadmill inclining to 10 degrees, it declined to -10 degrees. The exoskeleton applied the adaptive biomimetic torque throughout the trials. Participants were instrumented with Vicon markers to capture their kinematics, which were then used to establish ground truth estimates for phase, phase rate, stride length, and inclination. We computed the stride-wise RMSEs for both EKF phase and EKF phase rate, and raw errors for stride length and incline. We then compared the phase RMSEs to the RMSEs from the state-of-the-art TBE approach, and tested for significance against the TBE approach using a t-test.

#### F. Real-world Test

Finally, we wanted to characterize the ability of the EKF-based controller to adapt its estimates and torque assistance in a highly irregular outdoor environment. The same subject from H3 walked with the EKF-controlled exoskeleton on the Michigan Wave Field, which features a sinusoidal hill pattern of inclines and declines (from approximately  $30^\circ$  to  $-30^\circ$ ) and has been previously used to test the stability of bipedal robots [29]. This location was chosen to ‘stress-test’ the EKF in an environment that featured conditions outside its training dataset. The subject self-selected his gait patterns and route throughout the trial on the Wave Field, which is representative of the non-steady-state conditions that could occur in a practical setting. We recorded HD video of this trial and compared the recorded events to the EKF’s estimates to assess the adaptations to the Wave Field’s features. To obtain ‘ground truth’ phase values, we analyzed the video to determine the timings of HS events; we then interpolated phase values between them. As in H3, we performed a pairwise t-test comparing the differences in phase RMSE of EKF to TBE, using manually curated HS events double-checked against the video.

## IV. RESULTS

TABLE I  
TREADMILL TEST RESULTS

	Subject 1	Subject 2	Subject 3
EKF Phase RMSE (%)	3.3 (2.6)	4.0 (3.5)	4.1 (4.7)
EKF Phase Rate RMSE (%/s)	2.6 (1.8)	2.4 (5.3)	5.3 (24.4)
Stride Length Error (m)	-0.35 (0.13)	-0.11 (0.17)	-0.14 (0.22)
Incline Error (deg)	-1.8 (2.3)	-1.9 (2.3)	-2.8 (2.8)
TBE Phase RMSE (%)	56.1 (180.7)	71.1 (133.9)	109.5 (296.3)

#### A. Cross-Validation of EKF Performance

Our results support Hypothesis 1—that the EKF significantly outperforms TBE during an *in silico* leave-one-out cross validation. The phase RMS error for the EKF ( $1.53\% \pm 0.79\%$ ) was significantly lower ( $p = 1.3e - 40$ ) than the RMS error for the TBE estimator ( $2.09\% \pm 1.90\%$ ). The standard deviation of phase RMSE was more than twice as large for TBE than EKF, indicating that large phase estimation errors were more common with TBE. Additionally, our EKF predicted stride length with error  $0.039 \text{ m} \pm 0.11 \text{ m}$  and ramp inclination with error  $0.028^\circ \pm 1.43^\circ$ .

The second cross-validation test supported Hypothesis 2—that including ramp estimation in the EKF significantly improves phase estimation when compared to an EKF that does not feature ramp estimation. Another *in silico* cross-validation found the phase RMS error for the No-Ramp condition ( $1.67\% \pm 0.94\%$ ) under-performed the phase RMS error for the standard EKF condition to a statistically significant degree ( $p = 1.7e - 40$ ).

#### B. Treadmill Test

Hypothesis 3—that the EKF significantly outperforms TBE while applying torques for the treadmill experiment—is supported by Fig. 4 and the data in Tab. I. For all three subjects, the EKF significantly outperformed the conventional TBE approach. The standard deviation of phase RMSE was several times larger for TBE than EKF, indicating again that large phase estimation errors were much more common with TBE. Our EKF’s phase RMSE (cross-subject average  $3.8\% \pm 3.7\%$ ) is comparable to the best online phase estimation performance achieved in hip exoskeletons [14], which used machine learning to estimate phase for subjects walking through circuits that featured different ramps (phase RMSE  $5.04\%^3$ ). The EKF clearly captures the pulse-like change in phase rate during the fast 1.8 m/s and slow 0.8 m/s sections of the trials. The EKF simultaneously provided live estimates of both stride length and inclination (cross-subject average stride length error  $-0.11 \text{ m} \pm 0.18 \text{ m}$ , cross-subject average incline error  $-2.2^\circ \pm 2.5^\circ$ ). The EKF clearly responded to the changes in ground inclination, with a mean ramp error magnitude comparable to recent results from an offline ML-based sensor fusion approach, albeit with relatively higher variation [25] (absolute incline error  $1.25^\circ \pm 0.15^\circ$ ). The EKF was less responsive to changes in stride length, with changes occurring during the slow 0.8 m/s trials but stride length estimates staying relatively constant during the fast 1.8 m/s section of the trials.

#### C. Real-world test

Similarly, the EKF was superior to TBE during the non-steady-state Wave Field trial in which the subject self-selected a path and gait through the terrain with exoskeleton assistance ( $3.73\% \pm 2.22\%$  for the former,  $32.9\% \pm 38.3\%$  for the latter,  $p = 5.3e - 9$ ). The EKF state estimates and resulting adaptive torque from the Wave Field trial indicate that steps continue to be tracked in extreme conditions and that desired torque is changing according to the stride length and ramp angle (Fig. 5). To aid in analysis, we also show four stills that correspond to notable events from the trial; in particular, the position of the subject’s right foot is useful to demonstrate that the EKF is updating its ramp estimate correctly. A supplemental video of the Wave Field experiment is available for download.

The EKF captured all of the subject’s steps throughout his path, as shown in the plot of phase vs time and as verified through the video analysis. In addition to providing excellent phase estimation, the EKF was also able to adapt its task variable estimates in the face of the unsteady terrain as the subject walked. For example, anecdotally during the trial, the subject verbalized that he was intentionally slowing down and taking smaller steps prior to walking on an uphill portion of the Wave Field, to maintain stability. Accordingly, the EKF is able to capture this behavior in the task variables, noticeably decreasing the phase rate and stride length estimates when significant positive ramps occur (for example, at time D). The EKF’s adaptation of its state estimates is also reflected in the assistance from the exoskeleton. The biomimetic torque profile broadly increased the

<sup>3</sup>Note that comparing RMSE across distinct experiments is not a direct comparison of methods.

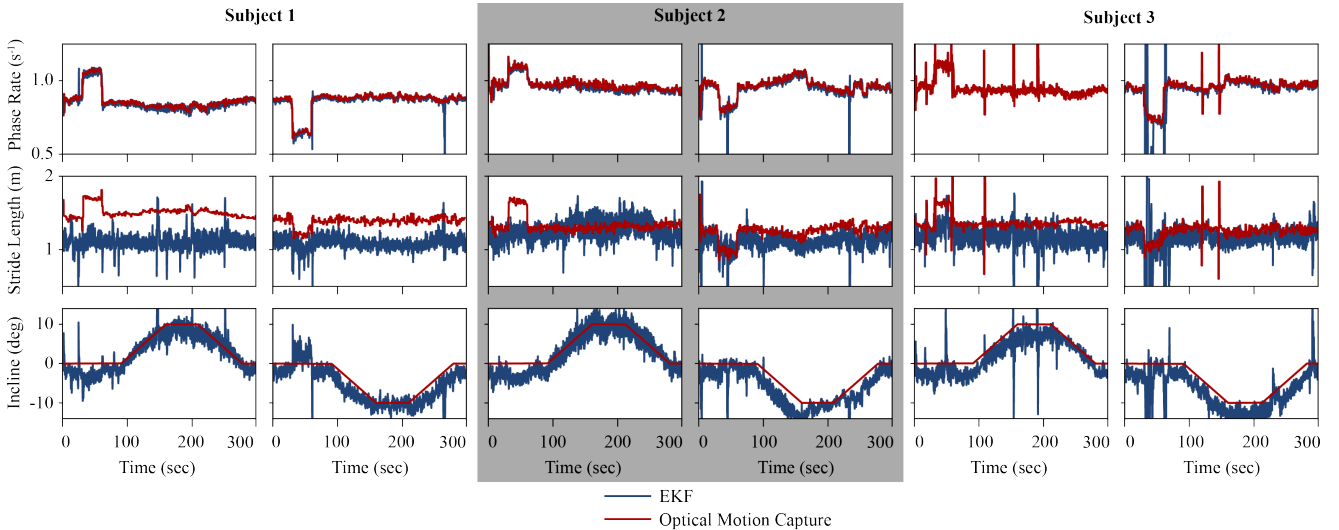


**Fig. 4.** State estimates from the live treadmill trials. Phase rate is shown in the first row, stride length in the second, and incline in the third. Overall, the EKF had excellent tracking of phase rate (and thus, phase), while adequately tracking inclination. The EKF was less responsive to changes in stride length, in part due to individualized differences in gait when compared to the trained gait model.

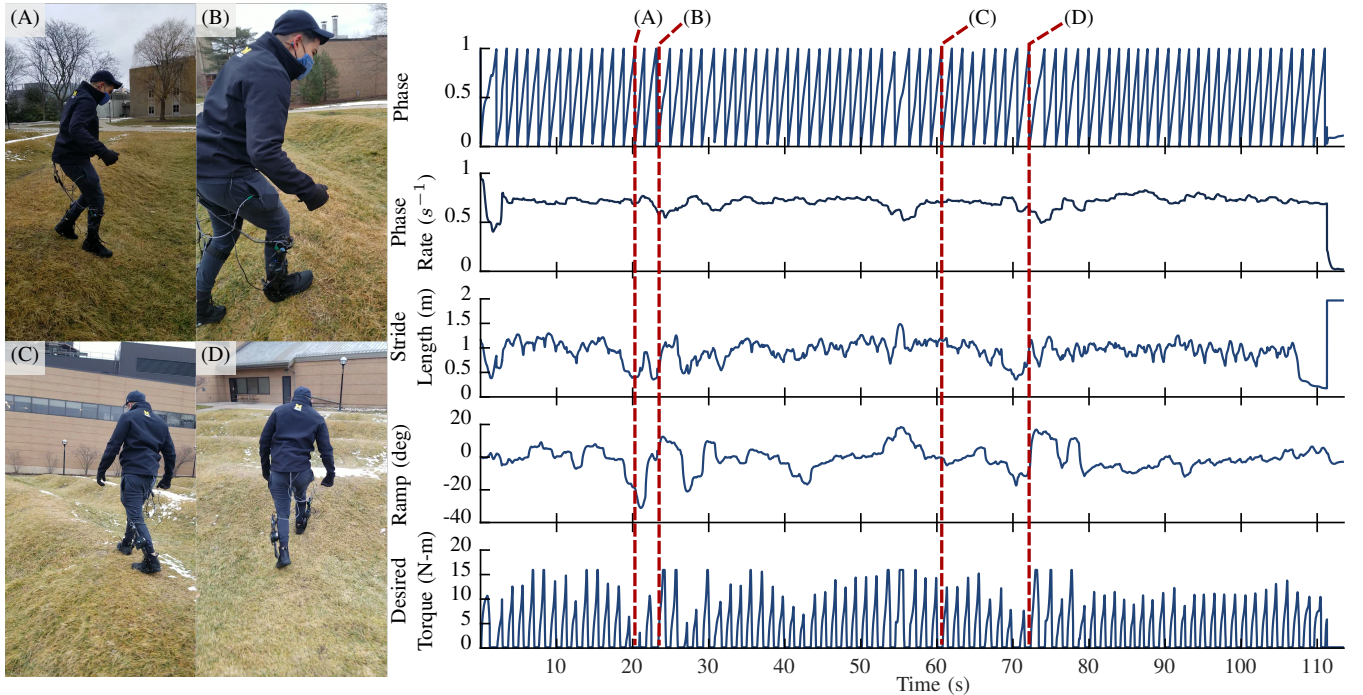


**Fig. 5.** Stills from the analyzed video taken during the Wave Field trial, with a focus on the EKF's ramp estimation performance. (A) The subject taking a declined stride, with the EKF correctly updating its estimate. (B) The subject walking up an incline, during one of the trial's three backup plan overrides throughout the trial. (C) The subject walking on a relatively flat portion of the Wave Field. (D) The subject going up another incline.

magnitude of its torque assistance when ground inclination was positive, and decreased it was negative. This trend is reflected in the torque shown in Fig. 5; where the EKF estimates positive ramps, torque rises, and where the EKF estimates negative ramps, torque decreases. Finally, the HS-based backup plan only engaged three times, at 2.10, 23.24 (see Fig. 5.B), and 111.30 seconds, indicating for the majority of the trial, the EKF was performing well.

## V. DISCUSSION

As expected, our EKF phase estimator outperformed the simple TBE estimator, with significantly lower phase RMSEs in the *in silico* steady-state treadmill trials. Fundamentally, the EKF observes the

behavior between heel-strikes, allowing it to better predict the phase variability that accompanies natural human walking, even in this steady-state test with a constant belt speed.

The presence of real-time ramp estimation within the EKF also significantly improved phase estimation. This is likely due to the ramp feature accounting for part of the variation from the kinematic sensor measurements, and therefore reducing the prediction errors. Without ramp estimation, modeling error increased, resulting in greater variance in the phase estimation signal.

In the non-steady-state treadmill experiment, the EKF estimator's advantage over the TBE increased substantially. This is explained by the non-steady-state trial featuring larger changes to the stride

length and step rate. Since the TBE approach estimates gait phase using past data collected roughly every second, it is unable to immediately update its estimates as conditions change. However as these parameters evolve, the EKF is still able to track the pattern in the global angles and infer how this pattern is changing. This allows it to predict future HS events and reduce its phase error when compared to the *a posteriori* HS-based phase signal.

In the Wave Field stress test, the EKF estimator maintained its significant advantage over the TBE as in the treadmill trial. The TBE featured its poorest performance during the Wave Field trial (up to 32.9% from 2.09% RMSE in the steady-state cross-validation trials), due to the highly variable nature of the terrain. In contrast, the EKF only experienced a phase RMSE increase of 2.2% during this trial compared to the cross-validation trials. Additionally, the HS-based backup estimator only activated three times during the entire two-minute trial, demonstrating that the EKF was functioning correctly in real-time for the vast majority of the task. More specifically, the backup engaged once at the start of the trial, once at the end of the trial, and once after slowing down while ascending a ramp (Fig. 5.B).

Using an EKF confers several advantages for our adaptive torque controller. Because our simple gait model predicts angles and velocities in a fundamentally structured way, we are able to encode a large, continuous class of locomotion tasks. The EKF equations are intuitive to understand and simple to implement on hardware, while still yielding comparable phase estimation performance to more complex machine learning approaches. Furthermore, the data-driven model component at the core of our controller may be easier to debug than so-called ‘black-box’ models that directly estimate gait parameters or control commands from sensor data. Our explicit gait model also allows us to be agnostic to the choice of exoskeleton hardware on which our controller is implemented; the hardware need only produce measurements of the human’s kinematics, which obviates the need for any separate hardware-specific sensor data collection on which to train a controller. The extreme conditions of the Wave Field test also demonstrated that our EKF controller can perform well even with tasks that were outside our training dataset.

Our EKF can also scale well to additional sensors. In our current implementation, we only use two sensors, along with their derivatives, but it would be straight-forward to implement other sensors, such as instrumented insoles, to further improve phase estimation. We can use the current dataset to regress relationships between these sensors’ measurements and our gait-state and simply extend the measurement vector in our EKF. We expect that this will further improve phase estimation due to the new information available from these sensors.

To further improve our estimates, we would first target the inter-person variability that dominates the model fit errors [24]. Every person walks differently, and this inter-person kinematic variation increases the variance of not only the estimated phase, but also the remaining state vector elements. This discrepancy due to inter-person variability is exemplified in Subject 1’s stride length estimates in Fig. 4. The consistently large error in Subject 1’s stride length estimate is due to his shank kinematics differing significantly from what the gait model predicts (Fig. 6 A). Subject 1’s actual measured kinematics (green) are closest to those predicted by the EKF model prediction (solid blue) using a far lower stride length (roughly 1.1 m) than the subject’s actual stride length (roughly 1.4 m). The gait model prediction using the actual stride length yields a poorer fit (transparent blue), thus the EKF underestimates the true stride length. Simple gait personalization techniques have been shown to significantly reduce the error in gait models over a continuous range of tasks [30], so we suspect that the variance of estimated phase could be reduced with such a personalized model.

Modeling error also arises from our use of piecewise Bernstein

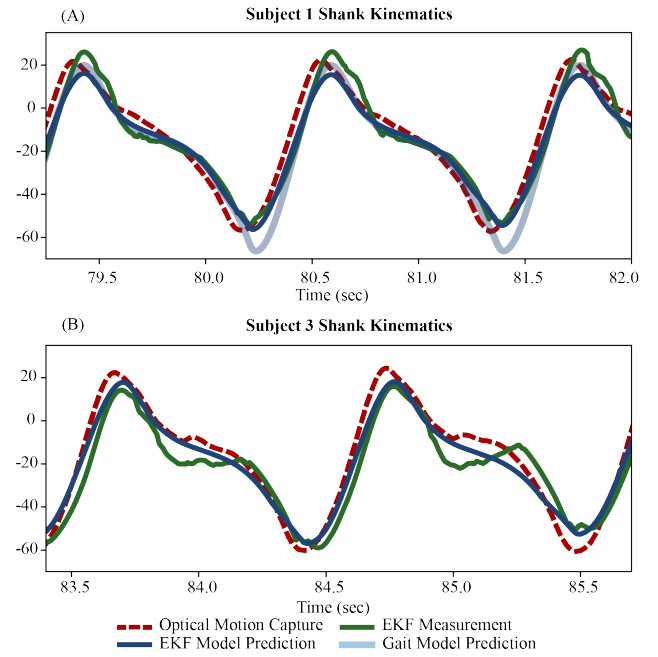


**Fig. 6.** (A) Subject 1’s shank kinematics during the treadmill trials, as an example of how inter-person gait variability can lead to errors in state estimation. Based on the subject’s measured kinematics (green), the EKF gait model predicts shank angles (solid blue) that imply a state estimate which underestimates the subject’s actual stride lengths; the gait model predictions using a stride length closer to the subject’s actual strides (transparent blue) are a poorer fit to Subject 1’s actual kinematics. (B) Subject 3’s shank kinematics during the treadmill trials, as an example of how the exoskeleton’s actuation during mid-stance disturbs the shank angle measurements. During mid-stride (evident at  $\sim 83.75$  and  $\sim 84.75$  seconds), this disturbance causes the shank measurement (green) to deviate significantly from the gait model estimates (blue), which leads to greater fluctuations in the state estimate.

polynomials to relate phase to foot and shank angles. The segmentation was chosen by inspection to allow a small number of parameters, but more generally, models in the style of a Fourier series allow us to determine how many parameters are worthwhile [23], [24]. Similarly, our model’s linear relationship with ramp and stride length could be enhanced with a more complex, nonlinear relationship, which may better represent how shank and foot angles actually vary with these task parameters. Future work can investigate the tradeoff between model complexity and accuracy to improve overall estimation.

Because the dataset used to regress our gait model only contained steady walking data, other tasks such as running or start/stopping are not explicitly modeled. While in theory the presented EKF can account for sudden stops by estimating  $\dot{p}$  as zero, we believe the estimator will benefit from training with data including such gait transitions (*e.g.*, [31]). As datasets grow to include more behaviors, our intention is to extend our continuous gait model with new task variables representing these other dimensions of human locomotion.

Unmodeled dynamics can also negatively impact our EKF performance. In particular, the exoskeleton’s actuation imposes a disturbance on the system through the physical deflection of the device’s IMU, which can lead to incorrect measurements of the shank angle. Our gait and heteroscedastic noise models assume that the measured shank angles will take on a specific, average profile; due to the exoskeleton’s actuation, the shank profiles that are actually measured are fundamentally different than what our models expect (Fig. 6B). When comparing the gait model’s prediction of what shank angle should look like (solid blue) to the exoskeleton’s measurements of

shank angle (green line), the discrepancy due to actuation during mid-stance is evident; the measurements have a significantly lower value compared to what the gait model predicts. While our EKF was sufficiently robust to these periodic disturbances for the majority of the trials, in some cases, our EKF was aggressive enough that these disturbances caused rapid, 'spike'-like changes in the state vector (most noticeable during Subject 3's trials). This required the heel-strike backup plan to engage and increased the variance of our state vector estimates relative to comparable machine-learning based techniques [14], [25]. As a potential solution, we can implement a model of the exoskeleton's compliance to account for these deflections, which may enable more aggressive EKF tuning and a faster response. Alternatively we may tune the EKF to reduce its bandwidth, which will reduce its response time but render it more robust to these disturbances.

In terms of the hardware implementation, our estimation quality is in part limited by the sample rate of our microcontroller, as a lower sample rate yields less information into the EKF. A lower sample rate thus limits the viable process noise gains we can choose for a functional EKF, and these would then tend to be conservative. Our EKF was implemented in Python on a Raspberry Pi 4, which resulted in a middling refresh rate (roughly 100 Hz). Future controllers that we develop will instead use Python extension modules that wrap faster C++ code to increase our sampling rate and bolster the performance of our EKF.

Finally, the live Wave Field trial was only conducted with a single participant. Although the results were promising, this sample may not be representative of the broader able-bodied human population. Future work will feature a greater sample size to ensure that our EKF controller is generalizable to the broader population as suggested by our *in silico* cross-validation results with 10 able-bodied human subjects.

## VI. CONCLUSION

We developed an exoskeleton torque controller based on an EKF which estimates phase, phase rate, stride length, and ramp in real time. This controller yields significantly reduced phase estimation errors compared to the state-of-the-art. Furthermore, this controller improves upon the state-of-the-art by allowing the assistive torque profile to adapt in real time in response to the state estimates. To the authors' knowledge, we are the first to estimate the gait phase variable along with stride length and ground inclination in real time and throughout an outdoor non-steady-state locomotion task. This result represents a meaningful milestone for practical exoskeleton control and usage outside the laboratory.

## APPENDIX I EXTENDED KALMAN FILTER IMPLEMENTATION

Starting from the state estimate at the previous time  $\hat{x}_{k-1|k-1}$  and the previous state covariance estimate  $P_{k-1|k-1}$ , our EKF implementation computes the current state estimate update using measurement  $z_k$ , dynamic model  $f(\cdot)$ , and measurement model  $h'(\cdot)$ . The process involves two steps. First, we propagate the (conveniently linear) dynamics from (16) across the time step,

$$\begin{aligned}\hat{x}_{k|k-1} &= F\hat{x}_{k-1|k-1}, \\ P_{k|k-1} &= FP_{k-1|k-1}F^T + \Sigma_Q.\end{aligned}$$

We then correct the estimate based on the measurement  $z_k$  as

$$\begin{aligned}\hat{x}_{k|k} &= \hat{x}_{k|k-1} + K_k(z_k - h'(\hat{x}_{k|k-1})), \\ P_{k|k} &= P_{k|k-1} - K_k H_k P_{k|k-1},\end{aligned}$$

where  $K_k = P_{k|k-1} H_k^T \left[ H_k P_{k|k-1} H_k^T + \Sigma_{R_k}(\hat{p}_{k|k-1}) \right]^{-1}$ ,

and  $H_k = \frac{\partial h'}{\partial x}|_{\hat{x}_{k|k-1}} \begin{pmatrix} 1 & 0 & 0 & 0 \\ 0 & 1 & 0 & 0 \\ 0 & 0 & \frac{dl}{dt_p} & 0 \\ 0 & 0 & 0 & 1 \end{pmatrix}.$

## REFERENCES

- [1] L. M. Mooney, E. J. Rouse, and H. M. Herr, "Autonomous exoskeleton reduces metabolic cost of walking," *Conf Proc IEEE Eng Med Biol Soc*, vol. 11, no. 1, pp. 3065–3068, 2014.
- [2] J. Zhang, P. Fiers, K. A. Witte, R. W. Jackson, K. L. Poggensee, C. G. Atkeson, and S. H. Collins, "Human-in-the-loop optimization of exoskeleton assistance during walking," *Science*, vol. 1284, no. June, pp. 1280–1284, 2017.
- [3] Y. Ding, M. Kim, S. Kuindersma, and C. J. Walsh, "Human-in-the-loop optimization of hip assistance with a soft exosuit during walking," *Science Robotics*, vol. 3, no. 15, pp. 1–9, 2018.
- [4] F. A. Panizzolo, G. M. Freisinger, N. Karavas, A. M. Eckert-Erdheim, C. Siviy, A. Long, R. A. Zifchock, M. E. LaFiandra, and C. J. Walsh, "Metabolic cost adaptations during training with soft exosuit assisting the hip joint," *Scientific Reports*, vol. 9, no. 1, pp. 1–10, 2019.
- [5] G. S. Sawicki, O. N. Beck, I. Kang, and A. J. Young, "The exoskeleton expansion: Improving walking and running economy," *Journal of NeuroEngineering and Rehabilitation*, vol. 17, no. 1, pp. 1–9, 2020.
- [6] K. E. Gordon and D. P. Ferris, "Learning to walk with a robotic ankle exoskeleton," *Journal of biomechanics*, vol. 40, no. 12, pp. 2636–2644, 2007.
- [7] T. Lenzi, M. C. Carrozza, and S. K. Agrawal, "Powered hip exoskeletons can reduce the user's hip and ankle muscle activations during walking," *IEEE Transactions on Neural Systems and Rehabilitation Engineering*, vol. 21, no. 6, pp. 938–948, 2013.
- [8] H. Zhu, C. Nesler, N. Divekar, V. Peddinti, and R. Gregg, "Design principles for compact, backdrivable actuation in partial-assist powered knee orthoses," *IEEE/ASME Trans. Mechatronics*, 2021.
- [9] M. R. Tucker, J. Olivier, A. Pagel, H. Bleuler, M. Bouri, O. Lamberg, J. del R Millán, R. Riener, H. Vallery, and R. Gassert, "Control strategies for active lower extremity prosthetics and orthotics: a review," *Journal of neuroengineering and rehabilitation*, vol. 12, no. 1, 2015.
- [10] M. A. Holgate, T. G. Sugar, and A. W. Bohler, "A novel control algorithm for wearable robotics using phase plane invariants," *IEEE Int. Conf. Robotics and Automation*, pp. 3845–3850, 2009.
- [11] D. Quintero, D. J. Villarreal, D. J. Lambert, S. Kapp, and R. D. Gregg, "Continuous-Phase Control of a Powered Knee-Ankle Prosthesis: Amputee Experiments Across Speeds and Inclines," *IEEE Trans. Robotics*, vol. 34, no. 3, pp. 686–701, 2018.
- [12] S. Rezazadeh, D. Quintero, N. Divekar, E. Reznick, L. Gray, and R. D. Gregg, "A Phase Variable Approach for Improved Rhythmic and Non-Rhythmic Control of a Powered Knee-Ankle Prosthesis," *IEEE Access*, vol. 7, pp. 109840–109855, 2019.
- [13] I. Kang, P. Kunapuli, and A. J. Young, "Real-Time Neural Network-Based Gait Phase Estimation Using a Robotic Hip Exoskeleton," *IEEE Trans. Medical Robotics and Bionics*, vol. 2, no. 1, pp. 28–37, 2019.
- [14] I. Kang, D. Molinaro, S. Duggal, Y. Chen, P. Kunapuli, and A. Young, "Real-time gait phase estimation for robotic hip exoskeleton control during multimodal locomotion," *IEEE Robotics and Automation Letters*, vol. 6, no. 2, pp. 3491–3497, 2021.
- [15] K. Seo, Y. J. Park, J. Lee, S. Hyung, M. Lee, J. Kim, H. Choi, and Y. Shim, "RNN-based on-line continuous gait phase estimation from shank-mounted IMUs to control ankle exoskeletons," *IEEE Int. Conf. Rehabilitation Robotics*, pp. 809–815, 2019.
- [16] N. Thatte, T. Shah, and H. Geyer, "Robust and adaptive lower limb prosthesis stance control via extended kalman filter-based gait phase estimation," *IEEE Robotics and Automation Letters*, vol. 4, no. 4, pp. 3129–3136, 2019.
- [17] H. Huang, F. Zhang, L. J. Hargrove, Z. Dou, D. R. Rogers, and K. B. Englehart, "Continuous locomotion-mode identification for prosthetic legs based on neuromuscular-mechanical fusion," *IEEE Trans. Biomedical Engineering*, vol. 58, pp. 2867–2875, 2011.

- [18] A. J. Young, A. M. Simon, N. P. Fey, and L. J. Hargrove, "Classifying the intent of novel users during human locomotion using powered lower limb prostheses," *Int IEEE EMBS Conf Neural Eng*, pp. 311–314, 2013.
- [19] C. D. Joshi, U. Lahiri, and N. V. Thakor, "Classification of gait phases from lower limb EMG: Application to exoskeleton orthosis," *IEEE Point-of-Care Healthcare Technologies*, pp. 228–231, 2013.
- [20] A. J. Young and L. J. Hargrove, "A classification method for user-independent intent recognition for transfemoral amputees using powered lower limb prostheses," *IEEE Trans. Neural Syst. Rehabilitation Eng.*, vol. 24, no. 2, pp. 217–225, 2016.
- [21] M. Liu, F. Zhang, and H. H. Huang, "An adaptive classification strategy for reliable locomotion mode recognition," *Sensors*, vol. 17, no. 9, 2017.
- [22] B. Hu, A. M. Simon, and L. Hargrove, "Deep generative models with data augmentation to learn robust representations of movement intention for powered leg prostheses," *IEEE Trans. Medical Robotics and Bionics*, vol. 1, no. 4, pp. 267–278, 2019.
- [23] K. R. Embry, D. J. Villarreal, R. L. Macaluso, and R. D. Gregg, "Modeling the Kinematics of Human Locomotion over Continuously Varying Speeds and Inclines," *IEEE Trans. Neural Syst. Rehabilitation Eng.*, vol. 26, no. 12, pp. 2342–2350, 2018.
- [24] K. R. Embry and R. D. Gregg, "Analysis of continuously varying kinematics for prosthetic leg control applications," *IEEE Trans. Neural Syst. Rehabilitation Eng.*, vol. 29, pp. 262–272, 2021.
- [25] J. Camargo, W. Flanagan, N. Csomay-Shanklin, B. Kanwar, and A. Young, "A Machine Learning Strategy for Locomotion Classification and Parameter Estimation Using Fusion of Wearable Sensors," *IEEE Transactions on Biomedical Engineering*, vol. 68, no. 5, pp. 1569–1578, 2021.
- [26] D. J. Villarreal, H. A. Poonawala, and R. D. Gregg, "A robust parameterization of human gait patterns across phase-shifting perturbations," *IEEE Trans. Neural Syst. Rehabilitation Eng.*, vol. 25, no. 3, pp. 265–278, 2017.
- [27] P. Malcolm, W. Derave, S. Galle, and D. De Clercq, "A Simple Exoskeleton That Assists Plantarflexion Can Reduce the Metabolic Cost of Human Walking," *PLoS ONE*, vol. 8, no. 2, pp. 1–7, 2013.
- [28] R. L. Medrano, G. C. Thomas, E. J. Rouse, and R. D. Gregg, "Extended kalman filter gait state estimation using a powered ankle exoskeleton: Adapting to changes in ramp and stride length [Source Code]," 2021. [Online]. Available: <https://doi.org/10.24433/CO.1404637.v1>
- [29] X. Da, R. Hartley, and J. W. Grizzle, "Supervised learning for stabilizing underactuated bipedal robot locomotion, with outdoor experiments on the wave field," in *IEEE Int. Conf. Robotics and Automation*, 2017, pp. 3476–3483.
- [30] E. Reznick, K. Embry, and R. D. Gregg, "Predicting Individualized Joint Kinematics over a Continuous Range of Slopes and Speeds," *Proc IEEE RAS EMBS Int Conf Biomed Robot Biomechatron*, pp. 666–672, 2020.
- [31] E. Reznick, K. Embry, R. Neuman, E. Bolivar-Nieto, N. P. Fey, and R. D. Gregg, "Lower-limb kinematics and kinetics during continuously varying human locomotion," <https://figshare.com/s/3d4f7d8641d8b0f81b77>, 2021.